



Large-scale preparation of UV photo-crosslinked composite membrane with high pervaporation desalination properties and excellent fouling resistance

Dujian Qin^{a,b}, Hangmin Liu^{a,b}, Jiahua Yan^a, ZiJian Yu^a, Zhongxiao Du^a, Bing Cao^{a,**}, Rui Zhang^{a,*}

^a College of Chemical Engineering, Beijing University of Chemical Technology, Beijing, 100029, China

^b College of Materials Science and Engineering, Beijing University of Chemical Technology, China

ARTICLE INFO

Keywords:

Pervaporation desalination
Spray-coating
UV photo cross-linking
Anti-fouling
Scale-up preparation

ABSTRACT

In this study, we developed a high-performance composite membrane with rapid cross-linking and large-scale technology for PV desalination. Some strategies were adopted to achieve this purpose. First, photo cross-linking was used to shorten the cross-linking time of PVA within 60 s. Second, a PTFE microfiltration membrane was utilized as the substrate that mitigated the transport resistance of the supporting layer. Third, an large-scale spray-coating device was built-up which completed the amplification preparation of composite PV membrane. Finally, ZIF-8 nano-particle was introduced into the PVA layer that increased the free volume and amorphous region of PVA, enhancing the water flux of membrane. When desalted a 3.5 wt% NaCl solution at 80 °C, a water flux of 307.58 ± 15.09 kg/m²·h was achieved for the PVA/ZIF-8/PTFE composite membrane. To better reflect the membrane performance, the permeance of PVA/ZIF-8/PTFE membrane was also calculated, which was reached to 674.37 kg/m² h bar, exceeding 18.4% than the highest reported property of PVA/PAN nanofiber membrane (569.55 kg/m² h bar). In addition, the composite membrane showed stable water flux and salt rejection when treating highly concentrated brine solution containing organic pollutant. When desalinated a 10 wt% NaCl solution with 1 wt% HA at 80 °C, the PVA/ZIF-8/PTFE membrane produced water with low conductivity of 15.78 µs/cm and a high water flux of 129.95 kg/m²·h in a period of 180 min.

1. Introduction

Water scarcity is one of the most critical challenges to human society [1–3]. To address this challenge, developing innovative desalination strategies that can harvest fresh water from seawater, brine and wastewater are indispensable [4–6]. Today, the main desalination technologies are multi-stage flash distillation (MSF), multi-effect distillation (MED) and reverse osmosis (RO) [7,8]. Nevertheless, MSF and MED are limited to be utilized in petroleum resources-rich areas [9], due to their inferior characteristics such as large equipment investment and high energy consumption [10]. On the other hand, RO occupies 60% of desalination market, because it has the superiority of low energy consumption (2–4 kWh/m³), simple operation et al. [11]. However, RO is not a proper technology for treating concentrated salt solutions because of the high osmosis pressure [12]. Membrane distillation (MD) has good tolerance to high salinity [13], while the problems of pore wetting and

fouling are the Achilles' heel for MD [14–16]. Very recently, it has been demonstrated that the wetting and fouling problems can be mitigated by pervaporation (PV) composite membrane [17]. Moreover, the energy consumption of PV can be reduced to the same level as RO by utilizing low quality heat sources [18]. (e.g., factory waste heat, latent heat of water vaporization) [19,20]. PV desalination has a great application prospect in desalting highly concentrated brine solutions [21–23].

Among all reported PV desalination membranes, PVA based composite membranes show superior desalination properties. Whereas some factors that limit their industrialization. First, crosslinking of PVA based membrane is often time-consuming (>2 h) [24–26]; second, water flux is still lower for employing [27]; last, large-scale preparation of PV membranes is seldom studied. To address these issues, some key strategies have been developed in this work. First, UV (ultraviolet) photo cross-linking method was adopted to crosslink the PVA layer within 60 s. Second, four substrates including: polyvinylidene fluoride (PVDF)

* Corresponding author.

** Corresponding author.

E-mail addresses: bciao@mail.buct.edu.cn (B. Cao), zhangrui1@mail.buct.edu.cn (R. Zhang).

<https://doi.org/10.1016/j.memsci.2023.122175>

Received 26 July 2023; Received in revised form 4 October 2023; Accepted 14 October 2023

Available online 5 November 2023

0376-7388/© 2023 Published by Elsevier B.V.

ultrafiltration membrane [28], polysulfone (PSF) membrane [29], electro-spun polyacrylonitrile (PAN) [30] nanofiber mat, and polytetrafluoroethylene (PTFE) micro-filtration membrane were compared for selecting an appropriate substrate. PTFE membrane was chosen for because of its large pore size and high porosity was positive to the gas flux following a viscous flow model [31]. Third, the photo cross-linking technology and spraying process were assembled together, realizing the preparation of composite PV membrane in large area.

However, PVA still contains numbers polar hydroxyl groups, which can form intermolecular or intramolecular hydrogen bonding [32]. This render the PVA crystallize easily and arrange molecular segments tightly, resulting in the water vapor molecules diffusion unfavourable [33]. To further improving the membrane permeability, the porous nanoparticles of ZIF-8 [34] was introduced into the PVA layer. ZIF-8 weaken the interaction between PVA and nanoparticles [35], thus making the PVA chain segments more loosely, which eventually increase the free volume but reduce the crystallinity of PVA layer. This regenerated large “vacant holes” indicated that water molecules could pass through the more free volumes [36]. Therefore, when desalting a 3.5 wt % NaCl feed solution at 80 °C, a super high water flux of 307.58 ± 15.09 kg/m²·h was obtained. Also, the permeance of PVA/ZIF-8/PTFE membrane was calculated, which was reached to 674.37 kg/m² h bar, exceeding 18.4% than the highest reported property of PVA/PAN nanofiber membrane (569.55 kg/m² h bar) [37]. In addition, when treating a 10 wt% NaCl water solution containing 1 wt% humic acid (HA) at 80 °C, the water flux gradually decreased from 152.68 to 129.95 kg/m²·h with a low conductivity of contributing water (<15.78 μs/cm) in operation time of 180 min. After washed by a 200 ppm NaClO water solution for 0.5 h, water flux could be recovered by 95.6%, showing the composites had excellent anti-fouling ability.

2. Experimental section

2.1. Materials and methods

PTFE microfiltration membrane was bought from Membrane solutions' Technology (China) Co., LTD. 15 wt% PVA-SBQ (a photo PVA cross-linked by UV, polymerization degree:1700, saponification degree (DS): 88%, concentration of SBQ: 0.03~0.05 mol/kg) solution was bought from Shanghai Guangyi Printing Equipment Technology Co., Ltd. Humic acid (HA, containing 90% fulvic acid) was purchased from Kmart Chemical Technology Co., Ltd (Tianjin). Sodium chloride (NaCl, purity ≥99.5%) was got from Sinopharm Chemical Reagent Co., Ltd. (China). Deionized (DI) water was supplied by a lab-equipped Millipore ultrapure water system. Zn(NO₃)₂·6H₂O (purity: 98%) and 2-methylimidazole (purity: 99%) were provided by Sigma-Aldrich. All chemicals were used as received without further treatment and purification.

2.2. Synthesis of ZIF-8 nanoparticle

For rapidly synthesizing the ZIF-8 materials, a typical aqueous solution method was adopted [34]. Specially, 3.95 mmol Zn(NO₃)₂·6H₂O (1.17 g in 8 g DI water) was added into a solution of 2-methylimidazole (22.70 g, 276.50 mmol) in 80 g DI water. After stirring the mixture solution at room temperature for 5 min. The nano-particles and solution was separated by centrifugation at 8000 rpm for 30 min. The obtained products were washed by DI water for at least 3 times, and then collected after drying at 40 °C overnight.

2.3. Spray-coating of the PTFE based composite membrane

Two aqueous solution containing 0.6 wt% PVA and 0.6 wt% PVA/ZIF-8 (10/3, wt/wt) were spray-coated onto a PTFE membrane. The auto-spraying apparatus set-up shown in Figs. S3a–c comprised an automatic guide rail, which can automatically regulate the reciprocating motion of the spraying gun (WA-101-102P, nozzle diameter: 1.0 mm), a

columniform rolling (length: 100.0 cm, diameter: 40.0 cm) that attaches to the PTFE substrate, and an industrial grade air compressor (Fujiwara, 7.5 kw) to provide the working spraying air. In spraying process, the movement speed of the spraying gun was set at 50 mm/s, and the rotational speed of columniform rolling was 40 rpm/min. The distance of the spraying gun to the membrane surface and the air pressure were set at 15 cm and 4.0 bar, respectively. The quantity of the spraying solution to the PTFE membrane was controlled at 51.9 μL/cm² for depositing a defect-free top layer consisting of pure PVA or PVA/ZIF-8. After coating, the PVA/PTFE and PVA/ZIF-8/PTFE composites were exposed to a 365 nm UV light at a power density of 90 mw/cm² for 60 s to crosslink PVA.

2.4. Characterization

2.4.1. Characterization of PVA based membrane

Fourier transform infrared spectroscopy (ATR-FTIR, Nicolet 560, USA) was used to characterize the chemical structure of membranes. The degrees of crystallinity were determined by X-ray diffraction analysis (XRD, Rigaku, Japan; CuK, λ = 0.15406 nm) using a MDI Jade 6 software. The samples were tested in an angle region from 5° to 90° with a scanning speed of 5°/min. The glass transition temperature were measured using a dynamic mechanical analyzer (DMA, Q800, USA). The free volume properties were analyzed by bulk positron annihilation lifetime spectroscopy (PALS) [38], a detailed testing method was introduced in the Supplementary information.

2.4.2. Determining the membrane morphology and contact angle

The surface and cross-section morphology was studied by a scanning electron microscope (SEM, HITACHI S-7800, Japan). The membrane surfaces were directly observed from the SEM images while the sample was fractured in liquid nitrogen to observe the cross-sectional morphology. A Nano measurement software-image J was used to estimate the thicknesses of dense PVA layer. Water contact angles of the PTFE, PVA/PTFE and PVA/ZIF-8/PTFE membranes were measured using a contact angle goniometer (DSA100, KRUSS, Germany) [39]. In each measurement, 2 μL droplets of DI water or n-Hexadecane was carefully dropped onto membrane surface and then using a high-speed optimum video analysis system to determine the dynamic contact angle. The contact angle was the average value of five replicates at random locations of membrane sample. The interface energy(γ) of these membrane was calculated by Owens method and Wu'hamonic mean method [40,41].

2.4.3. Desalination properties of the membrane under vacuum mode

The desalination properties were analyzed using a bespoke apparatus as reported in Ref. [42], applying a pressure of 100 Pa at the membrane permeate side, as shown in Fig. S15. For PTFE MD, the desalination testing under vacuum (V) mode named as VMD, for PVA sprayed PTFE composite PV membrane, the testing named as VPV. The permeated water vapor was collected in a liquid nitrogen cold trap and then weighed to calculate water flux using eq (1):

$$J_w = \frac{\Delta m}{A \times t} \quad (1)$$

where J_w was the permeate flux (kg/m²·h); Δm (kg) was the weight gain over time; A was the effective membrane area (m²), which was 3.8 cm²; and t was the data operation period (h). During the tests, 3.5 wt% NaCl water solution was circulated on membrane feed side at velocity of 0.1 m/s, and the feed temperature were maintained at 40 °C–80 °C. To estimate the salt rejection performance, an electrical conductivity meter (DDSJ-308F, Leichi, China) was used to determine the salt concentrations of feed and permeate solutions using eq (2):

$$R = \left(\frac{C_f - C_p}{C_f} \right) \times 100\% \quad (2)$$

where R was the salt rejection rate of these membranes, C_f and C_p were the salt concentrations of the feed and permeate solutions, respectively. These equations were also used to calculate the water flux and salt rejection of these membranes when treating 10 wt% NaCl aqueous solution.

2.4.4. Desalination properties of the membrane under a direct contact mode

In order to alleviate the mass transfer resistance caused by the accumulation effect of water vapor at the permeable side of membrane [43,44], a direct-contact (DC) mode in this experiment was adopted by omitting the vacuum pumps or sweeping gas device [45] but replacing a thermostatic coolant (20.2 ± 0.7 °C) at membrane permeate side (Fig. S16). For PTFE MD, the DC testing named as DCMD, for PVA sprayed PTFE composite PV membrane, the DC testing named as DCPV. 600 mL DI water was used as the liquid coolant while 2 L, 3.5 wt% or 10 wt% NaCl water solution was served as feed. The hot NaCl water solution at membrane feed side and the cold water stream (20.2 ± 0.7 °C) at permeate side were circulated at the same speed of 0.14 m/s using two peristaltic pumps (WT600S, frei fluid technology co. LTD, China). The conductivity of contributing water of permeate solutions were measured by a conductivity meter (DDSJ-308F, Leichi, China) that recorded the conductivity every hour. The contributing water at the membrane permeate side was weighted using an electrical balance (CP2102, OHAUS) and used to calculate the membrane flux using eq (1). The effective transport area of membrane was 22.5 cm^2 and the system was first operating for 0.5 h before recording data to stabilize the feed and coolant temperatures.

2.4.5. Anti-fouling properties of the PTFE and PVA/ZIF-8/PTFE membranes

Fouling behaviors of the PTFE and PVA/ZIF-8/PTFE membranes were estimated by desalting a 10 wt% NaCl solution with 1 wt% HA (acting as an organic contaminant) at 80 °C using the vacuum mode. The membrane fluxes were calculated using eq (1) and the conductivity of gaining water over time was monitored by the conductivity meter (DDSJ-308F, Leichi, China). To maintain a constant concentration, certain amount of DI water was added to the feed solution every 2 h during the testing. Moreover, the anti-fouling performance of these membranes were embodied by the water flux recovery ratio (FRR) calculating using eq (3) [46]:

$$FRR = \left(\frac{J_0}{J_t} \right) \times 100\% \quad (3)$$

where J_0 was the initial water flux, J_t was the water flux of the polluted membranes after washing. The polluted membranes were washed for 0.5 h using a 200 ppm NaClO water solution.

3. Result and discussion

3.1. Selection of cross-linking method for separating layer

The preparation of separation layer can greatly affect the efficiency of membrane production, so it is necessary to choose a appropriate way for cross-linking the separating layer. At the beginning of our previous study, the thermal treating method (Fig. S1a) is directly used to cross-link PVA layer for its convenience. However, the process is long, which would take more than 2 h [24]. Subsequently, this process is shortened to 15 min via introducing acid catalyst into the cross-linking system (Fig. S1b) [37]. But the accelerated process is still too long to meet the demand of rapid membrane preparation. With research development and cognitive advancement, PVA cross-linking process further speed up to 60 s, which is achieved by the UV photo-curing method [47]. Fig. 1 shown the reaction process, the C=C bonds of photo cross-linked PVA was broken by UV light and then formed a four C-C ring. The cross-linking structure was confirmed by FTIR in Fig. 2. The reduction of peak area at 1624 cm^{-1} assigned to C=C bond were 0%, 92.2%, 95.0%, 96.4% and 99.6% at a curing time of 0 s, 5 s, 15 s, 30 s and 60 s, respectively (the reaction conversion was calculated as eq S1). The cross-linking accomplished within 60 s. Therefore, for preparing the separating layer quickly, the UV photo-curing technology was selected.

3.2. Selection of the PTFE substrate

Porous substrate played a key role in achieving high performance of composite pervaporation (PV) membrane [27,29]. This was because the porous structure reduced the problem of water vapor accumulation at the interface between substrate and separating layer [30]. Therefore, for acquiring a PV membrane with high performance, a appropriate substrate was necessary to select. Table S1 shown that PTFE possessed the largest mean pore radius and electro-spun PAN nanofiber mat had the

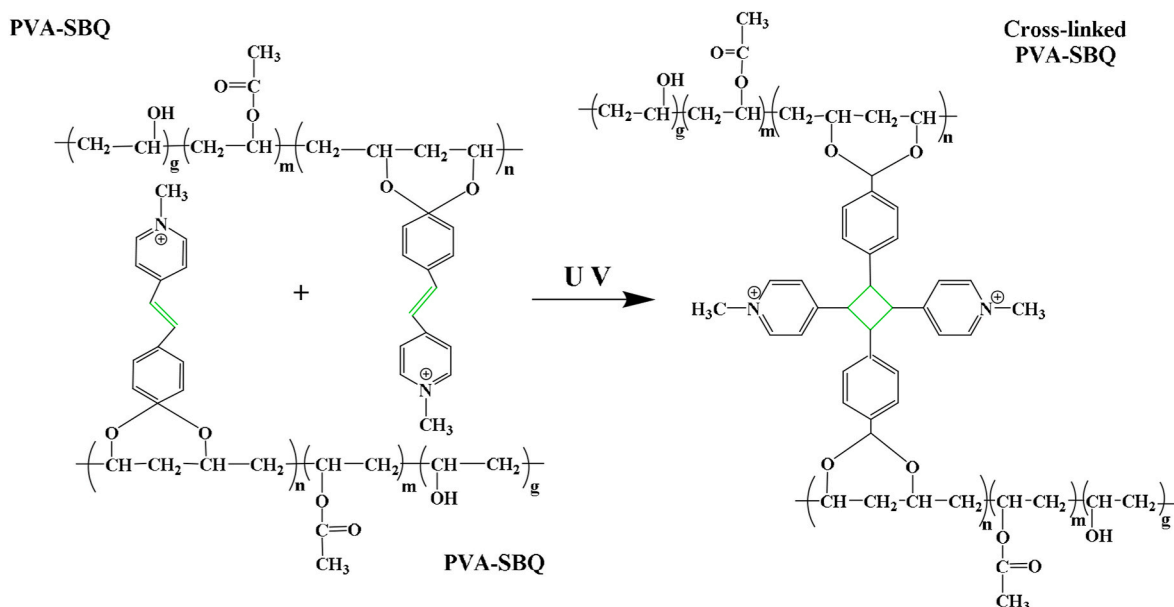


Fig. 1. Schematic diagrams of the PVA crosslinking process by UV crosslinking.

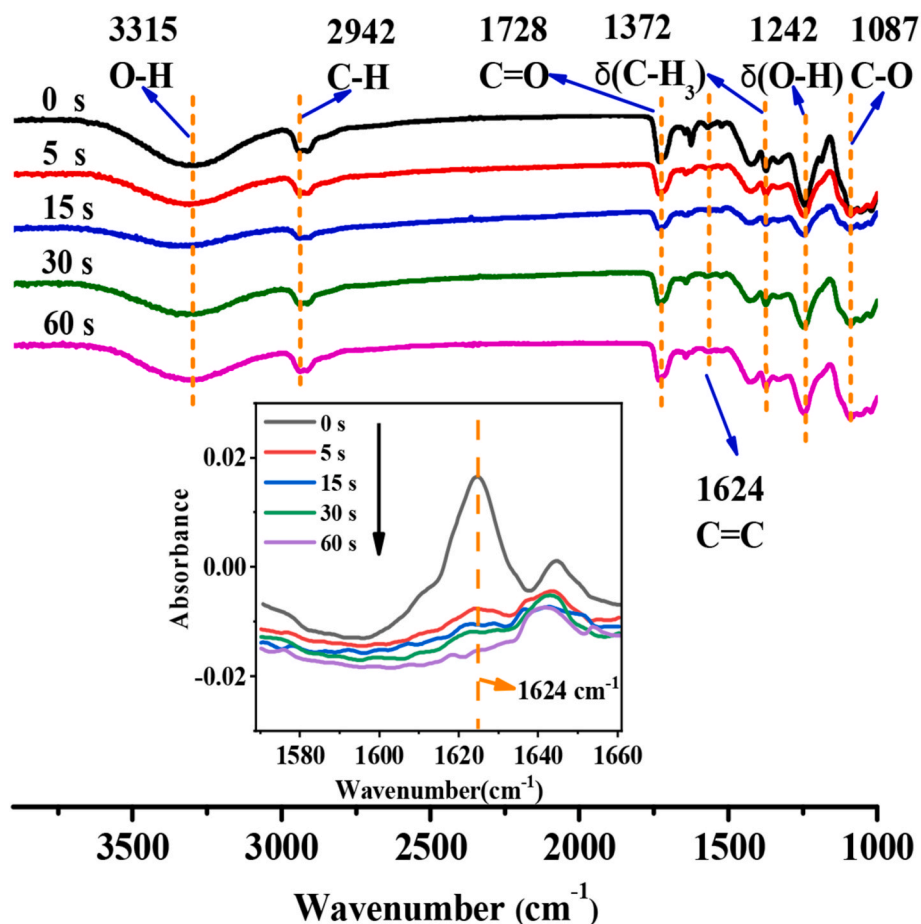


Fig. 2. The FTIR spectra of PVA over varied cross-linking time.

highest porosity than the membrane fabricated by the non-solvent induced phase inversion method like PVDF and PVDF. Following a viscous flow model, the gas flux of porous substrate was positive to membrane pore surface size and porosity as described in the Poiseuille equation [31]. Clearly, PTFE and electrospinning mat were suitable. But the process of electrospinning mat was complexity and time-consuming, which was not easy to scale-up. Therefore, PTFE membrane was chosen.

3.3. Fabricating the PVA/PTFE composite membrane

The above work completed the selection of cross-linking method for separating layer and the selection of substrate. But constructing a PVA layer on hydrophobic PTFE membrane was challenged by dripping or scraping method (PTFE has interface incompatibility with the PVA water solution). Spray-coating technology solved the problem of PVA/PTFE delamination [48] and was adopted for preparing the composites. Fig. S3 shown the assembled setting up and the preparation process of large area membrane. Specifically, as shown in Fig. S4, at the driving force of compressed air, PVA droplets formed. Some droplets deposited at the PTFE surface and other droplets penetrated the random grids lapped by the PTFE fibers under the extrusion of the spray-solution. At the same time, the automatic spraying gun moved back and forth following the motor direction to let the PVA droplets spray at the PTFE membrane (touching onto the roller surface) in large area. After spraying, the sprayed PVA layer was exposed in photo cross-linking light for cross-linking. Because of the constructed layer, PTFE accomplished the transition of porous MD to dense PV composite membrane successfully. Thus, no gas could pass through (Fig. S7) and no liquid water could be squeezed out (Table S3). More importantly, this equipment helped us to fabricate a composite membrane with large area, which was

distinguished from the small experimental membrane.

3.4. Characterization of the membrane morphology

SEM morphology in Figs. S10a-f revealed that along with the increased spraying quantity of PVA solution, more and more pores on PTFE surface were covered by PVA. At the end of spraying, a smooth intact PVA layer with 1.2 μm thickness was formed on the rough surface of PTFE (Fig. S10j). The sprayed construction could be verified from the stripped surface morphology (stripping process shown in Fig. S11a). Large amount of PVA immersed into the PTFE pores and some polymers were wrapped around the PTFE filaments (Fig. S11b). Moreover, this packaging morphology could be observed obviously via fluorescent dyeing experiment. Fig. S11c demonstrated that PVA presented fluorescent green (PTFE fibers was gray), and this color contrast became increasingly clear along with the increment of PVA spraying. Ultimately a full fluorescent green PVA wrapped the PTFE fibers or covered the pores after spraying. In addition, by employing the electrochemical impedance spectroscopy [49], the infiltrated area of PVA was probed (more detail in Supporting Information, Section B.8). Fig. S14 showed the capacitance of membrane (equivalent area [50]) increased by an order of magnitude for the PVA/PTFE membrane compared with PTFE.

3.5. Desalination properties of the PTFE and PVA/PTFE membranes

Two testing methods including direct contact and vacuum mode were used to estimate the desalination performances. As Fig. 3a shown, in direct contact modes the water flux of PVA/PTFE was slowly dropped to 26.46 $\text{kg}/\text{m}^2\cdot\text{h}$ from 43.74 $\text{kg}/\text{m}^2\cdot\text{h}$ but maintained a stable conductivity of water production $<10.0 \mu\text{s}/\text{cm}$ for treating a 10 wt% NaCl

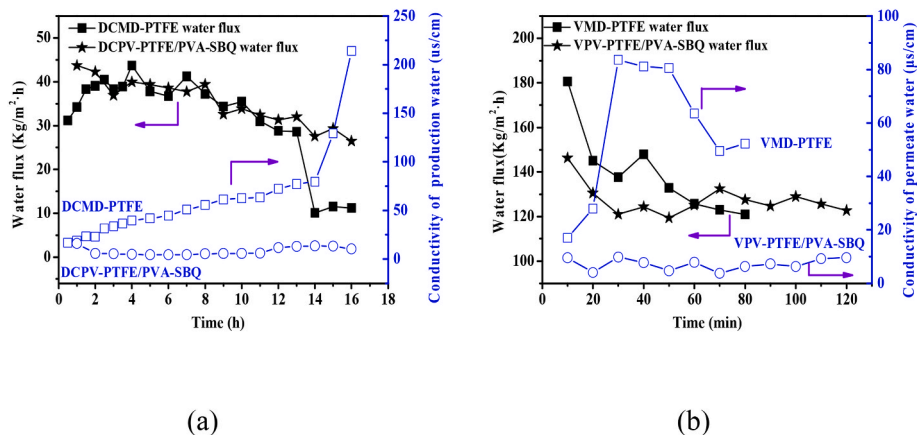


Fig. 3. Water flux and conductivity of permeate water:(a) PTFE, PVA/PTFE membranes measured at direct contact mode with 75.0 ± 1.1 °C, 10 wt% NaCl feed, (b) PTFE, PVA/PTFE at vacuum mode with 80 °C, 10 wt% NaCl feed.

solution for 16 h at 75 °C. By comparison, the water flux of PTFE increased from $31.14 \text{ kg/m}^2\cdot\text{h}$ to $45.74 \text{ kg/m}^2\cdot\text{h}$ within 4 h while the conductivity of contributing water rapidly increased to $39.8 \text{ }\mu\text{s/cm}$. After 16 h, the water flux reduced to $11.16 \text{ kg/m}^2\cdot\text{h}$ but the permeate water conductivity increased to $214.0 \text{ }\mu\text{s/cm}$. Clearly, the PTFE membrane was not stable during testing. The problem became severe as membrane operated in vacuum mode. Fig. 3b demonstrated that after a 80 min experiment, the water flux of PTFE reduced from $180.63 \text{ kg/m}^2\cdot\text{h}$ to $120.96 \text{ kg/m}^2\cdot\text{h}$ and the conductivity of the producing water increased to $52.3 \text{ }\mu\text{s/cm}$. Whereas for the PVA/PTFE, the conductivity of contributing water maintained at $9.6 \text{ }\mu\text{s/cm}$ and the water flux gradually decreased from $146.32 \text{ kg/m}^2\cdot\text{h}$ to $122.68 \text{ kg/m}^2\cdot\text{h}$ during a 120 min experiment. After testing testing by 80 °C, 10 wt% NaCl at vacuum mode, the difference became more clear. Fig. 4a demonstrated many NaCl crystals appeared on the PTFE membrane surface, and some NaCl crystals even immersed into the interior pores, thus wetting the PTFE. For the PVA/PTFE, a smooth surface with few NaCl crystals was observed, as shown in Fig. 4b.

Nevertheless, PTFE always displayed higher water flux than that of PVA/PTFE for desalting of a 3.5 wt% NaCl feed at temperatures from 40 °C to 80 °C whether in direct contact or vacuum mode (Fig. 5). The lower water flux would be attributed to the resistance of PVA layer. PVA molecular chains were tightly bounded together by arranging -OH [51, 52], and had a strong tendency to crystallization (Fig. S17), which was difficult to water diffuse [53]. Therefore, the layer needed to regulate.

3.6. Regulating the separation layer of PVA

The synthesized ZIF-8 nano-particles (average diameter 103.1 nm, Fig. S19) was introduced to further regulate the PVA layer structure and

the PVA/ZIF-8/PTFE was prepared. For treating the 3.5 wt% NaCl feed solution at 70 °C in vacuum mode, PVA/ZIF-8/PTFE membrane had a similar water flux of $226.58 \pm 3.16 \text{ kg/m}^2\cdot\text{h}$ with PTFE membrane ($217.95 \pm 8.08 \text{ kg/m}^2\cdot\text{h}$), as shown in Fig. 6a. This may be caused by two reasons: (1) MD pore wetting or contamination problems were happened, which would cause a rapid water flux reduction for PTFE [54, 55]; (2) membrane concentration polarization [56] led to the water concentration difference between the bulk feed solution and the solution at the membrane surface. To alleviate the above problems, these membranes were evaluated again using a 70 °C DI water as feed. Fig. 6b showed that the pure water flux of PTFE is $221.77 \pm 6.58 \text{ kg/m}^2\cdot\text{h}$, $213.48 \pm 8.82 \text{ kg/m}^2\cdot\text{h}$, $196.27 \pm 2.46 \text{ kg/m}^2\cdot\text{h}$ and $158.22 \pm 21.88 \text{ kg/m}^2\cdot\text{h}$ at a membrane back pressure of 100 Pa, 2000 Pa, 3000 Pa–4000 Pa, respectively. While for the PVA/ZIF-8/PTFE membrane, a water flux of $247.41 \pm 8.73 \text{ kg/m}^2\cdot\text{h}$, $221.19 \pm 11.35 \text{ kg/m}^2\cdot\text{h}$, $192.48 \pm 18.98 \text{ kg/m}^2\cdot\text{h}$ and $161.72 \pm 10.23 \text{ kg/m}^2\cdot\text{h}$ was observed. The PVA/PTFE membrane had the lowest water fluxes of $185.69 \pm 7.76 \text{ kg/m}^2\cdot\text{h}$, $167.72 \pm 5.30 \text{ kg/m}^2\cdot\text{h}$, $158.33 \pm 1.06 \text{ kg/m}^2\cdot\text{h}$ and $108.11 \pm 3.90 \text{ kg/m}^2\cdot\text{h}$. Hence, the ZIF-8 nano-particle improved the water flux.

The performance improvement can be understood from the free volume variation of PVA selective layer. Where the free volume could be finely divided into r_3 (smaller pore from the cross-linked site) and r_4 (larger pore from networks clusters as well as the polymer-filler interface) [57,58]. Results in Fig. 7a showed that r_3 of PVA/ZIF-8 film increased from 0.138 to 0.156 and r_4 increased from 0.297 to 0.431, respectively. The increment of r_3 was because of the well-dispersed ZIF-8 nano-particle effectively disrupted the PVA chains packing [59]. While enlarged r_4 was the weak interaction between PVA and nano-particle caused loose chain packing and an increased chain mobility at the particle-polymer interface [57,60]. This disrupting chains packing and

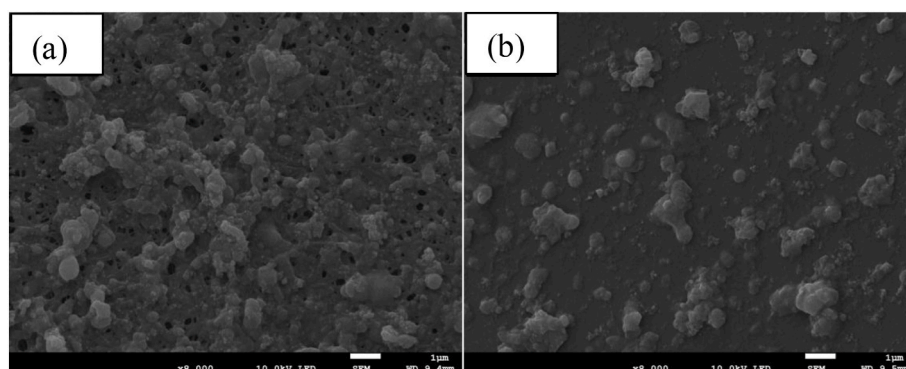


Fig. 4. SEM surface of PTFE (a) and PVA/PTFE (b) after testing by 80 °C, 10 wt% NaCl.

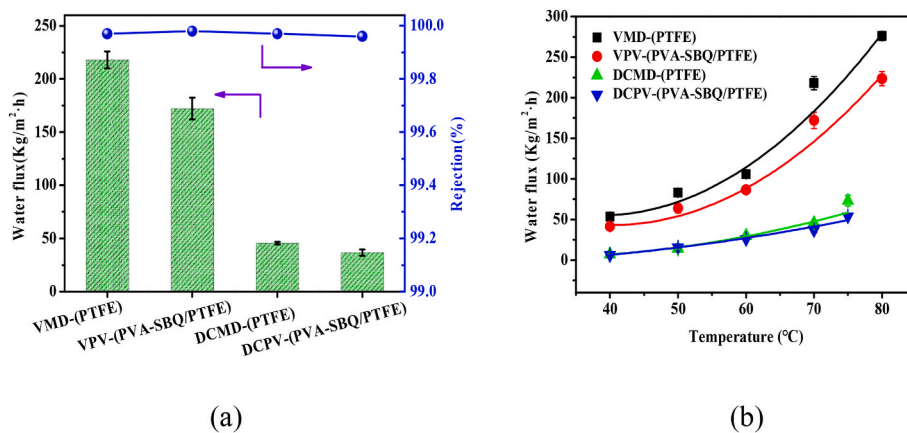


Fig. 5. (a) Water flux and NaCl rejection of PTFE (VMD, DCMD mode) and PVA/PTFE (VPV, DCPV mode) operated at 70 °C, 3.5 wt% NaCl feed; (b) Water flux of PTFE and PVA/PTFE varied feed temperature of 3.5 wt% NaCl feed.

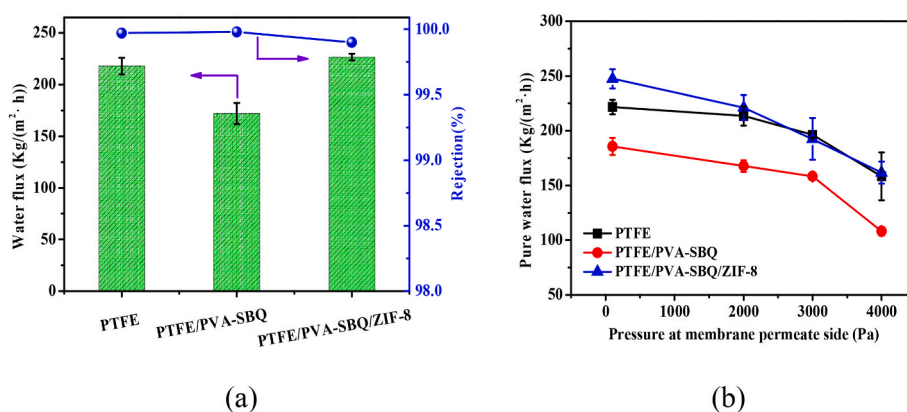


Fig. 6. (a) Water flux and NaCl rejection of PTFE, PVA/PTFE and PVA/ZIF-8/PTFE dealt 70 °C, 3.5 wt% NaCl feed at vacuum mode; (b) pure water flux of PTFE, PVA/PTFE and PVA/ZIF-8/PTFE using 70 °C DI water as feed by controlling the pressure at membrane back side.

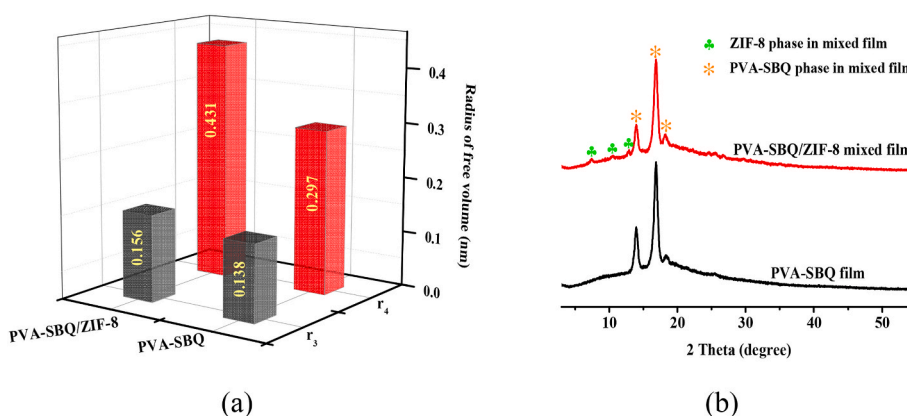


Fig. 7. The radius free volume (a), and XRD (b) of the PVA based membrane.

enhancing chains mobility could be confirmed by the decreased T_g , where the T_g of PVA and PVA/ZIF-8 film were 102.1 °C and 94.7 °C, respectively (Fig. S23a). This regenerated large “vacant holes” indicated that water molecules could pass through the more free volumes (Fig. S24) so that the water permeability was enhanced. Meanwhile, the performance improvement could also be understood from the crystallinity variation. Fig. 7b shows that the crystallinity reduced from 30.0% (PVA) to 15.2% (PVA/ZIF-8), implying enlarged amorphous regions of the PVA/ZIF-8 mixed matrix membrane, which was also beneficial for

diffusion [53].

3.7. Membranes performance and anti-fouling property

Membranes water flux performance of the PVA/ZIF-8/PTFE was assessed at 40 °C, 50 °C, 60 °C, 70 °C and 80 °C, using a 3.5 wt% NaCl feed solution. Fig. 8a presented the water flux of these membranes rapidly increased along with the rising feed liquid temperature. This was due to because the water vapor pressure at membrane feed side

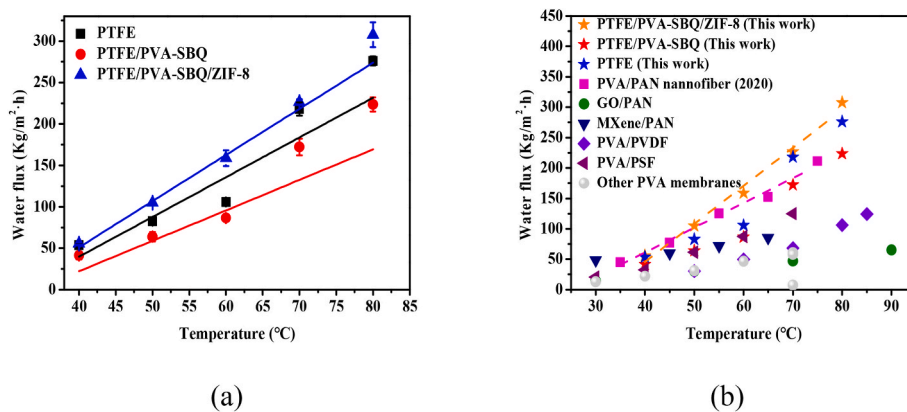


Fig. 8. (a) Water flux of PTFE, PVA/PTFE and PVA/ZIF-8/PTFE varied feed temperature of 3.5 wt% NaCl from 40 °C, 50 °C, 60 °C, 70 °C–80 °C at vacuum mode; (b) Water flux performance comparison of our membrane with other reported work.

exponentially grew based on the Arrhenius equation [61], so the rising feed temperature offered higher driving force to make more water molecules transfer across the membrane. Thus, a water flux of 307.58 ± 15.09 kg/m²·h was acquired at the feed temperature of 80 °C, as shown in Fig. 8b. To better reflect the membrane performance, the permeance and permeability were calculated as illustrated in Refs. [62,63]. Table 1 listed the comparison result of our membrane with literature-reported membranes, which the permeance of PVA/ZIF-8/PTFE membrane reached to 674.37 kg/m²·h bar, exceeding 18.4% than the permeance of PVA/PAN nanofiber membrane (569.55 kg/m²·h bar). And the permeability of our membrane was 7.96×10^{-4} kg/m²·h·bar, still more higher than that of PVA/PAN nanofiber membrane (4.16×10^{-4} kg/m²·h·bar), although the water flux of that membrane was 211.37 kg/m²·h when desalinated 3.5 wt% NaCl solution in 75 °C [37]. Besides, PVA/ZIF-8/PTFE membrane also displayed good anti-fouling property. Such as in the desalination of 10 wt% NaCl (inorganic contaminant)+1 wt% HA (organic contaminant) solution at 80 °C, the contributing water collecting at membrane back side consistently maintained a low conductivity <15.78 μs/cm, and the water flux slowly decreased from 152.68 kg/m²·h to 129.95 kg/m²·h during the operation period of 180 min. Whereas the conductivity of contributing water for PTFE membrane was increased quickly to 36.6 μs/cm in a very short time of 10 min (to 474 μs/cm in 90 min period), and the water flux dropped to 111.32 kg/m²·h from 153.32 kg/m²·h in 120 min, as shown in Fig. 9a.

The SEM images of the polluted membranes revealed this disparity visually. Fig. 10a demonstrated a large amount of sheet-like contaminants attached to PTFE membrane surface after completing the above test. Lots of irregular bulky contaminants still wrapped PTFE filament (Fig. 10c) after washing with a 200 ppm NaClO water solution for 0.5 h. By comparison, few small particles remained on the surface of PVA/ZIF-8/PTFE membrane after the desalination experiment (Fig. 10b), and the rough surface became smooth after the same washing process, as observed in Fig. 10d. Clearly, the PVA/ZIF-8 layer mitigated the contamination problem of the PTFE membrane. This was due to that the hydrophilic PVA/ZIF-8 layer had a higher surface energy property (Table S5) than the PTFE (Table S2). More obviously, this anti-fouling

ability could be embodied in the water flux recovery rate of membrane (FRR). The FRR of PTFE, PVA/ZIF-8/PTFE shown in Fig. 9b were 75.0%, 95.6% suggested that the water flux of the PTFE membrane returned to 75% after washing while that of PVA/ZIF-8/PTFE returned to 95.6%. This further confirmed that the PVA/ZIF-8 layer alleviated the contamination problem.

4. Conclusion

In this work, spraying-coating and UV photo cross-linking technique was adopted for a scale-up fabrication of a PV composite membrane. The cross-linking time of the PVA layer by photo curing was shortened to 60 s. And spray-coating solved the interface incompatibility between the PVA and the PTFE layers. In addition, the addition of ZIF-8 particles increased the free volumes (r_3 and r_4) and the amorphous region of the PVA layer, which favorable water transport. Therefore, when desalted a 3.5 wt% NaCl solution at 80 °C, a super highest water flux of 307.58 ± 15.09 kg/m²·h was achieved. The permeance of PVA/ZIF-8/PTFE membrane was also calculated, which was reached to 674.37 kg/m²·h bar, exceeding 18.4% than the highest reported property of PVA/PAN nanofiber membrane (569.55 kg/m²·h bar). The composite membrane had fine quality of the contributing water and stable water flux when desalted highly concentrated brine solutions. When desalinating a 10 wt% NaCl+1 wt% HA solution, a high water flux of 129.95 to 152.68 kg/m²·h with a low conductivity of contributing water (<15.78 μs/cm) in an operation time of 180 min was achieved. The excellent desalination property, stable producing water quality, outstanding anti-fouling ability, and the sale-up fabrication technology showed a great prospect for industrialization of the PV desalination membranes.

Notes

The authors declare no competing financial interest.

Table 1
The performance comparison between our membrane with literature-reported work.

Membrane	Thickness	Feed temp. (°C)	Salt conc. (wt%)	Flux (kg/m ² ·h)	Permeance (kg/m ² ·h·bar)	Permeability (kg·m/m ² ·h·bar)	Author
PTFE/PVA/ZIF-8	1.18 μm	80	3.5	307.58	674.37	7.96×10^{-4}	This work
PVA/PAN nanofiber	0.73 μm	75	3.5	211.37	569.55	4.16×10^{-4}	[37]
GO/PAN	~60 nm	90	3.5	65.1	96.36	5.78×10^{-6}	[1]
Mxene/PAN	~60 nm	65	3.5	85.4	354.50	2.13×10^{-5}	[2]
PVA/PVDF	0.88 μm	85	3.5	120.0	215.32	1.89×10^{-4}	[30]
PVA/PSF	0.61 μm	70	3.5	124.8	416.28	2.54×10^{-4}	[29]
Other PVA membrane	0.8 μm	70	3.5	46.3	154.44	1.24×10^{-4}	[31]

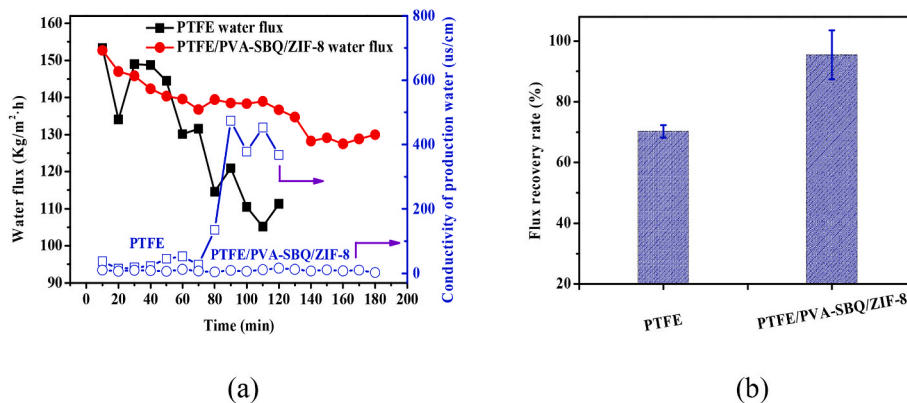


Fig. 9. (a) Water flux and conductivity of permeate water of PTFE and ZIF-8/PVA/PTFE after long-operation measurement by 80 °C, 10 wt% NaCl+1 wt% HA at vacuum mode, and (b) Flux recovery rate (FRR) of PTFE and PVA/ZIF-8/PTFE cleaning by 200 ppm NaClO solution 0.5 h.

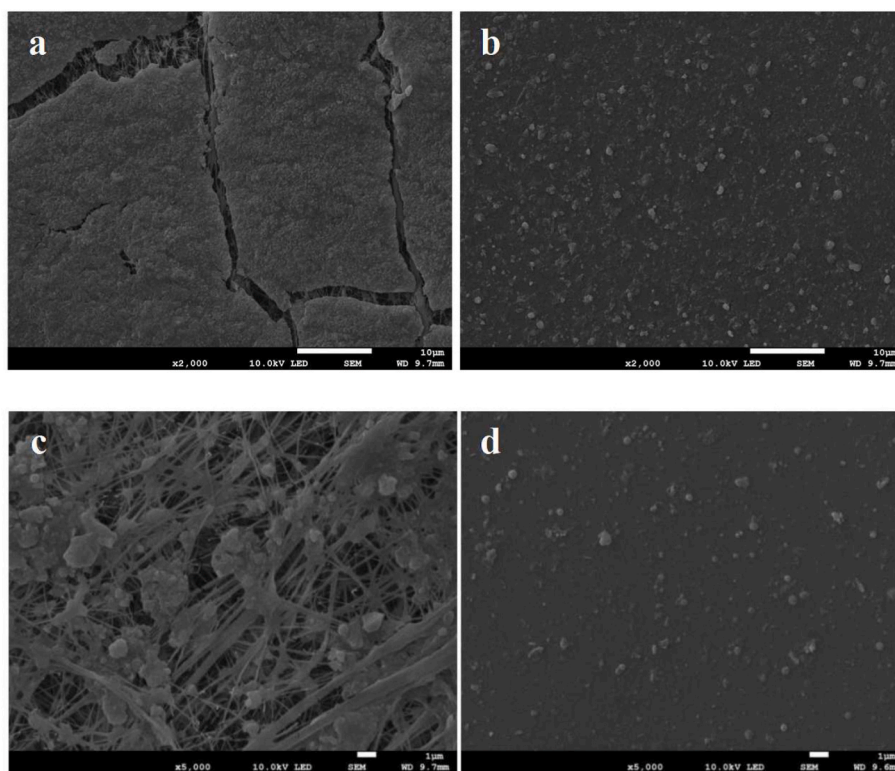


Fig. 10. Surface SEM of (a) PTFE and (b) PVA/ZIF-8/PTFE by long period testing by 80 °C, 10 wt% NaCl at vacuum mode; and surface SEM of (c) PTFE and (d) PVA/ZIF-8/PTFE after 200 ppm NaClO solution cleaning 0.5 h.

Declaration of competing interest

The authors declare that they have no known competing financial interests or personal relationships that could have appeared to influence the work reported in this paper.

Data availability

No data was used for the research described in the article.

Acknowledgments

This research is funded by National Key Research and Development Program (2021YFC01201-3).

Appendix A. Supplementary data

Supplementary data to this article can be found online at <https://doi.org/10.1016/j.memsci.2023.122175>.

References

- [1] W.W. Li, H.Q. Yu, B.E. Rittmann, Chemistry: reuse water pollutants, *Nature* 528 (2015) 29–31.
- [2] S.B. Grant, J.D. Saphores, D.L. Feldman, A.J. Hamilton, T.D. Fletcher, P.L.M. Cook, M. Stewardson, B.F. Sanders, L.A. Levin, R.F. Ambrose, A. Deletic, R. Brown, S. C. Jiang, D. Rosso, W.J. Cooper, I. Marusic, Taking the “waste” out of “wastewater” for human water security and ecosystem sustainability, *Science* 337 (2012) 681–686.
- [3] C.J. Vörösmarty, P.B. McIntyre, M.O. Gessner, D. Dudgeon, A. Prusevich, P. Green, S. Glidden, S.E. Bunn, C.A. Sullivan, C.R. Liermann, P.M. Davies, Global threats to human water security and river biodiversity, *Nature* 467 (2010) 555–561.

- [4] I. Ihsanullah, M.A. Atieh, M. Sajida, M.K. Nazala, Desalination and environment: a critical analysis of impacts, mitigation strategies, and greener desalination technologies, *Sci. Total Environ.* 780 (2021), 146585.
- [5] M.O. Mavukkandy, C.M. Chabib, I. Mustafa, A.A. Ghafri, F. AlMarzooqi, Brine management in desalination industry: from waste to resources generation, *Desalination* 472 (2019), 114187.
- [6] G. Amy, N. Ghaffour, Z. Li, L. Francis, R.V. Linares, T. Missimer, S. Lattemann, Membrane-based seawater desalination: present and future prospects, *Desalination* 401 (2017) 16–21.
- [7] J. Andrianne, F. Alardin, Thermal and membrane processes economics: optimized selection for seawater desalination, *Desalination* 153 (1–3) (2003) 305–311.
- [8] Z. Wang, T. Horseman, A.P. Straub, N. Yip, D. Li, M. Elimelech, S. Lin, Pathways and challenges for efficient solar-thermal desalination, *Sci. Adv.* 5 (2019), eaax0763.
- [9] O.A. Hamed, Evolutionary Developments of Thermal Desalination Plants in the Arab Gulf Region, Beirut Conference, 2004.
- [10] V.G. Gude, V. Fthenakis, Energy efficiency and renewable energy utilization in desalination systems, *Prog. Energy.* 2 (2020), 022003.
- [11] V.G. Gude, Energy consumption and recovery in reverse osmosis, *Desalination Water Treat.* 36 (2011) 239–260.
- [12] J. Rioyo, V. Aravinthan, J. Bundschuh, M. Lynch, A review of strategies for RO brine minimization in inland desalination plants, *Desalination Water Treat.* 90 (2017) 110–123.
- [13] Z. Yan, H. Yang, F. Qu, H. Yu, H. Liang, G. Li, J. Ma, Reverse osmosis brine treatment using direct contact membrane distillation: effects of feed temperature and velocity, *Desalination* 423 (2017) 149–156.
- [14] T. Horseman, Y. Yin, K.S.S. Christie, Z. Wang, T. Tong, S. Lin, Wetting, scaling, and fouling in membrane distillation: state-of-the-art insights on fundamental mechanisms and mitigation strategies, *ACS EST Engg* 1 (1) (2021) 117–140.
- [15] Z. Wang, S. Lin, Membrane fouling and wetting in membrane distillation and their mitigation by novel membranes with special wettability, *Water Res.* 112 (2017) 38–47.
- [16] Y. Yin, N. Jeong, T. Tong, The effects of membrane surface wettability on pore wetting and scaling reversibility associated with mineral scaling in membrane distillation, *J. Membr. Sci.* 614 (2020), 118503.
- [17] H. Zeng, S. Liu, J. Wang, Y. Li, L. Zhu, M. Xu, C. Wang, Hydrophilic SPEEK/PES composite membrane for pervaporation desalination, *Sep. Purif. Technol.* 250 (2020), 117265.
- [18] W. Kaminski, J. Marszałek, E. Tomczak, Water desalination by pervaporation-Comparison of energy consumption, *Desalination* 433 (2018) 89–93.
- [19] A. Cipollina, M.G. Di Sparti, A. Tamburini, G. Micale, Development of a Membrane Distillation module for solar energy seawater desalination, *Chem. Eng. Res. Des.* 90 (12) (2012) 2101–2121.
- [20] G. Dong, J.F. Kima, J.H. Kima, E. Drioli, Y.M. Lee, Open-source predictive simulators for scale-up of direct contact membrane distillation modules for seawater desalination, *Desalination* 402 (2017) 72–87.
- [21] R. Castro-Muñoz, Breakthroughs on tailoring pervaporation membranes for water desalination: a review, *Water Res.* 187 (2020), 116428.
- [22] A. Selim, A.J. Toth, D. Fozer, E. Haaz, Pervaporative desalination of concentrated brine solution employing crosslinked PVA/silicate nanoclay membranes, *Chem. Eng. Res. Des.* 155 (2020) 229–238.
- [23] J. Sun, X. Qian, Z. Wang, F. Zeng, H. Bai, N. Li, Tailoring the microstructure of poly (vinyl alcohol)-intercalated graphene oxide membranes for enhanced desalination performance of high-salinity water by pervaporation, *J. Membr. Sci.* 599 (2020), 117838.
- [24] R. Zhang, B. Liang, T. Qu, B. Cao, P. Li, High-performance sulfosuccinic acid cross-linked PVA composite pervaporation membrane for desalination, *Environ. Technol.* 40 (3) (2019) 312–320.
- [25] B. Liang, K. Pan, L. Li, E.P. Giannelis, B. Cao, High performance hydrophilic pervaporation composite membranes for water desalination, *Desalination* 347 (2014) 199–206.
- [26] L. Gautam, S.G. Warkar, S.I. Ahmad, R. Kant, M. Jain, A review on carboxylic acid cross-linked polyvinyl alcohol: properties and applications, *Polym. Eng. Sci.* 62 (2022) 225–246.
- [27] Q. Li, B. Cao, P. Li, Fabrication of high performance pervaporation desalination composite membranes by optimizing the support layer structures, *Ind. Eng. Chem. Res.* 57 (32) (2018) 11178–11185.
- [28] J. Meng, P. Li, B. Cao, High-flux direct-contact pervaporation membranes for desalination, *ACS Appl. Mater. Interfaces* 11 (2019) 28461–28468.
- [29] D. Qin, H. Liu, T. Xiong, J. Wang, R. Zhang, B. Cao, P. Li, Enhancing the property of composite pervaporation desalination membrane by fabricating a less resistance substrate with porous but skinless surface structure, *Desalination* 525 (2022), 115496.
- [30] D. Qin, R. Zhang, B. Cao, P. Li, Fabrication of high-performance composite membranes based on hierarchically structured electrospun nanofiber substrates for pervaporation desalination, *J. Membr. Sci.* 638 (2021), 119672.
- [31] R.W. Schofield, A.G. Fane, C.J.D. Fell, Gas and vapour transport through microporous membranes. I. Knudsen-Poiseuille transition, *J. Membr. Sci.* 53 (1–2) (1990) 159–171.
- [32] N. Chen, J. Zhang, The role of hydrogen-bonding interaction in poly (vinyl alcohol)/poly (acrylic acid) blending solutions and their films, *Chin. J. Polym. Sci.* 28 (2010) 903–911.
- [33] S. Van Nguyen, B.K. Lee, Polyvinyl alcohol/alkyl ketene dimer films with excellent water resistance and water vapor barrier properties, *Mater. Lett.* 307 (2022), 131045.
- [34] Y. Pan, Y. Liu, G. Zeng, L. Zhao, Z. Lai, Rapid synthesis of zeolitic imidazolate framework-8 (ZIF-8) nanocrystals in an aqueous system, *Chem. Commun.* 47 (2011) 2071–2073.
- [35] D. Yang, S. Yang, Z. Jiang, S. Yu, J. Zhang, F. Pan, X. Cao, B. Wang, J. Yang, Polydimethyl siloxane-graphene nanosheets hybrid membranes with enhanced pervaporative desulfurization performance, *J. Membr. Sci.* 487 (2015) 152–161.
- [36] Z. Si, J. Li, L. Ma, D. Cai, S. Li, J. Baeyens, J. Degève, J. Nie, T. Tan, P. Qin, The ultrafast and continuous fabrication of a polydimethylsiloxane membrane by ultraviolet-induced polymerization, *Angew. Chem. Int. Ed.* 131 (48) (2019) 17335–17339.
- [37] Y. Xue, J. Huang, C.H. Lau, B. Cao, P. Li, Tailoring the molecular structure of crosslinked polymers for pervaporation desalination, *Nat. Commun.* 11 (1) (2020) 1461.
- [38] H. Wu, X. Zhang, D. Xu, B. Li, Z. Jiang, Enhancing the interfacial stability and solvent-resistant property of PDMS/PES composite membrane by introducing a bifunctional aminosilane, *J. Membr. Sci.* 337 (1–2) (2009) 61–69.
- [39] C.L. Lai, R.M. Liou, S.H. Chen, G.W. Huang, K.R. Lee, Preparation and characterization of plasma-modified PTFE membrane and its application in direct contact membrane distillation, *Desalination* 267 (2–3) (2011) 184–192.
- [40] A.E. Bangerla, K. Appaiah, A conditional justification for the determination of surface energy of solids using contact angle methods, *Mater. Chem. Phys.* 234 (2019) 168–171.
- [41] F. Hejda, P. Solar, J. Kousal, Surface free energy determination by contact angle measurements -A comparison of various approaches, WDS'10 Proceedings of Contributed Papers (2010) 25–30. Part III.
- [42] P. Zhao, J. Meng, R. Zhang, B. Cao, P. Li, Molecular design of chlorine-resistant polymer for pervaporation desalination, *Sep. Purif. Technol.* 268 (2021), 118671.
- [43] R. Wang, S.L. Liu, T.T. Lin, T.S. Chung, Characterization of hollow fiber membranes in a permeator using binary gas mixtures, *Chem. Eng. Sci.* 57 (2002) 967–976.
- [44] H. Liu, L. Fu, H. Liu, C.L. Zhang, B. Cao, P. Li, Designing an atmosphere controlling hollow fiber membrane system for mango preservation, *Kor. J. Chem. Eng.* 34 (2017) 2019–2026.
- [45] E. Huth, S. Muthu, L. Ruff, J.A. Brant, Feasibility assessment of pervaporation for desalinating high-salinity brines, *J. Water Reuse Desalin.* 4 (2014) 109–124.
- [46] J. Zheng, M. Li, K. Yu, J. Hu, X. Zhang, L. Wang, Sulfonated multiwall carbon nanotubes assisted thin-film nanocomposite membrane with enhanced water flux and anti-fouling property, *J. Membr. Sci.* 524 (2017) 344–353.
- [47] J. Meng, P. Zhao, B. Cao, C.H. Lau, Y. Xue, R. Zhang, P. Li, Fabricating thin-film composite membranes for pervaporation desalination via photo-crosslinking, *Desalination* 512 (2021), 115128.
- [48] J. Meng, C.H. Lau, Y. Xue, R. Zhang, B. Cao, P. Li, Compatibilizing hydrophilic and hydrophobic polymers via spray coating for desalination, *J. Mater. Chem. A* 8 (2020) 8462.
- [49] C. Li, X. Li, X. Du, Y. Zhang, W. Wang, T. Tong, A.K. Kota, J. Lee, Elucidating the trade-off between membrane wetting resistance and water vapor flux in membrane distillation, *Environ. Sci. Technol.* 54 (2020) 10333–10341.
- [50] Q. Huang, Q. Luo, Z. Chen, L. Yao, P. Fu, Z. Lin, The effect of electrolyte concentration on electrochemical impedance for evaluating polysulfone membranes, *Environ. Sci. Water Res. Technol.* 4 (2018) 1145–1151.
- [51] N. Chen, J. Zhang, The role of hydrogen-bonding interaction in poly (vinyl alcohol)/poly (acrylic acid) blending solutions and their films, *Chin. J. Polym. Sci.* 28 (2010) 903–911.
- [52] E. Jia, L. Su, P. Liu, M. Jiang, G. Ye, J. Xu, Hydrogen bond and crystalline structure of the junction network in polyvinyl alcohol/dimethylsulfoxide gels, *J. Polym. Res.* 21 (9) (2014) 548.
- [53] S.V. Nguyen, B.K. Lee, Polyvinyl alcohol/alkyl ketene dimer films with excellent water resistance and water vapor barrier properties, *Mater. Lett.* 307 (2022), 131045.
- [54] H. Chamani, J. Woloszyn, T. Matsuura, D. Rana, C.Q. Lan, Pore wetting in membrane distillation: a comprehensive review, *Prog. Mater. Sci.* 122 (2021), 100843.
- [55] T. Horseman, Y. Yin, K.S.S. Christie, Z. Wang, T. Tong, S. Lin, Wetting, scaling, and fouling in membrane distillation: state-of-the-art insights on fundamental mechanisms and mitigation strategies, *ACS EST Engg* 1 (1) (2021) 117–140.
- [56] C. Shang, J. Xia, L. Sun, G.G. Lipscomb, S. Zhang, Concentration polarization on surface patterned membranes, *AIChE J.* 68 (2022), e17832.
- [57] G. Liu, W.S. Hung, J. Shen, Q. Li, Y.H. Huang, W. Jin, K.R. Lee, J.Y. Lai, Mixed matrix membranes with molecular-interaction-driven tunable free volumes for efficient bio-fuel recovery, *J. Mater. Chem. A* 3 (8) (2015) 4510–4521.
- [58] W. Liu, Y. Li, X. Meng, G. Liu, S. Hu, F. Pan, H. Wu, Z. Jiang, B. Wang, Z. Li, X. Cao, Embedding dopamine nanoaggregates into a poly (dimethylsiloxane) membrane to confer controlled interactions and free volume for enhanced separation performance, *J. Mater. Chem. A* 1 (11) (2013) 3713.
- [59] D. Yang, S. Yang, Z. Jiang, S. Yu, J. Zhang, F. Pan, X. Cao, B. Wang, J. Yang, Polydimethyl siloxane-graphene nanosheets hybrid membranes with enhanced pervaporative desulfurization performance, *J. Membr. Sci.* 487 (2015) 152–161.
- [60] M. Fang, C. Wu, Z. Yang, T. Wang, Y. Xia, J. Li, ZIF-8/PDMS mixed matrix membranes for propane/nitrogen mixture separation: experimental result and permeation model validation, *J. Membr. Sci.* 474 (2015) 103–113.
- [61] Y. Xu, C. Chen, J. Li, Experimental study on physical properties and pervaporation performances of polyimide membranes, *Chem. Eng. Sci.* 62 (9) (2007) 2466–2473.
- [62] Y. Li, E.R. Thomas, M.H. Molina, S. Mann, W.S. Walker, M.L. Lind, F. Perreault, Desalination by membrane pervaporation: a review, *Desalination* 547 (2023), 116223.
- [63] E.R. Thomas, A. Jain, S.C. Mann, Y. Yang, M.D. Green, W.S. Walker, F. Perreault, M.L. Lind, R. Verduzco, Freestanding self-assembled sulfonated pentablock

terpolymer membranes for high flux pervaporation desalination, *J. Membr. Sci.* 613 (2020), 118460.